Fluid Dynamic Analysis Inside a Solar Salts Prilling Power Using a Eulerian-Lagrangian Approach

Mauricio Lague[1], Abdiel Mallco[1], Mauro Henriquez[1], Magin Mendoza[1], Carlos Portillo[1], Carlos Soto[1], Carlos Duran[1], Gerardo Matamoros[1], Victor Tabilo[1], Abel Taquichiri[1]

[1]Centro de Desarrollo Energético Antofagasta (Chile)

Abstract

Solar thermal storage technology has undergone significant development in recent years, especially about the types of storage fluids through the search for new mixtures that offer greater performance and energy storage autonomy. On the other hand, there is a new problem which is the way to remove these salts for a new use, at the University of Antofagasta there is a small-scale system for emptying these salts stored in a small tank. The system consists of a tower in which a mixture of salt is sprayed at high temperature and solidified by means of a heat transfer process inside the tower in which air circulates at room temperature. This document shows the hydrodynamic analysis of these particles inside the tower, the air and the interaction between them and the surrounding fluid. The analysis is performed using a Eulerian-Lagrangian approach using the Ansys Fluent R18.1 Computational Fluid Dynamics package through a CFD-DPM coupling.

Keywords: Solar salt, prilling, CFD, DPM, particle interaction.

1. Introduction

Prilling is a granulation process, in which a molten material is sprayed by means of a sprinkler into a cooling medium, generally air, and solidifies into particles under the influence of surface tension and gravity, droplets that fall freely form an almost spherical shape (Saleh and Barghi, 2016). During the fall through the ascending air, the droplets will cool until they begin to solidify into fine particles, which is calculated using a shrunken non-solidified core model (Ricardo et al., 2013). The most widely used droplet formation mechanism is generally by jet formation, which is subsequently broken into droplets. These disintegration mechanisms are found as a function of the flow rate of the liquid (Dumouchel, 2008). Understanding and reproducing the behavior of the gas-solid flow through mathematical models is of great importance to properly design some of the specific equipment for this process. The gas-solid flow has been used in various areas of the processing industry such as power generation, in the drying of granulated materials, in the transport of particles, in the combustion of coal in fluidized bed and in the industry of the oil refining. (Paz-Paredes et al., 2017)

In this work, the fluid-dynamic behavior inside a molten salt prilling tower for the termosolar industry is analyzed (Fig. 1). Molten salts represent an important element within solar thermal storage systems in concentrating solar thermal plants, these fluids store energy in the form of heat to be used in periods of operation of the plant in the absence of the Sun, the most used fluid is the so-called solar salt or nitrate salt, which is a eutectic mixture of 60% sodium nitrate ($NaNO_3$) and 40% potassium nitrate (KNO_3). Nitrate salt is considered the most important element in thermal energy storage (TES). Although nitrates may be capable of operating at high temperatures, it is understood that these will not reach the temperatures necessary to achieve power cycle efficiency goals. The salts used must have favorable thermo-physical properties for heat transfer and energy storage (Mehos et al., 2017).

The mixture is stable in air and has a low vapor pressure, it also has a variation in density during the phase change to solid state of 4.6%. These salts can be used in a temperature range of 260°C to about 621°C. As the temperature decreases, the salts begin to crystallize at 238°C and solidify at 221°C.

doi:10.18086/swc.2021.36.01 Available at http://proceedings.ises.org

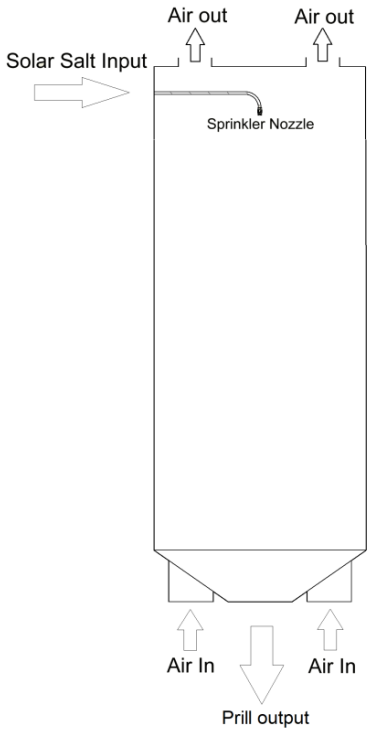

Fig. 1: Prilling tower diagram

Therefore, this work aims to study the fluid dynamic behavior of both the air (gas phase) that circulates inside this tower and the salt particles (discrete phase) that solidify as they descend through the tower. The study is carried out using a Eulerian approach for the gas phase and a Lagrangian approach for the discrete phase. These analyzes are carried out with the help of the Ansys Fluent 18.1 software using a coupled CFD-DPM model.

2. Process description

The analysis corresponds to the dynamic fluid behavior inside the tower shown in Fig. 1 where there is the entry of solar salt in liquid state at a temperature of 290°C and in which fine particles are obtained at the base of the tower of salt in solid state at a temperature of approximately 40°C. The tower operating conditions are shown in Tab. 2. While the properties of salt are shown in Tab.1

Tab. 1 Thermophysical properties of solar salt

Property	Value	Unit	Reference
Specific heat	1,520	J $kg^{-1}K^{-1}$	Mehos et al., 2017
Density	1,700	kg m^{-3}	Mehos et al., 2017
Melting/solidification point	220	°C	Mehos et al., 2017
Latent heat of solidification	161,000	J kg^{-1}	Nissen, 1980g

The tower is located at the University of Antofagasta-Chile in the Antofagasta Energy Development Center, and its main function is solidification into fine molten salt particles located in a $1m^3$ capacity thermal storage tank.

Tab. 2: Technical data and operating conditions of the tower

Parameter	Valor	Unidad
Tower section	2x2	m
Effective tower height	6.5	m
Inlet air velocity	12.5	m s^{-1}
Inlet salt flow	0.000056	m^3s^{-1}
Inlet salt velocity	9.161	m s^{-1}
Inlet salt temperature	290	°C
Salt outlet temperature	40	°C
Air inflow temperature	20	°C

The prills produced have a relatively uniform size of about 0.5 mm and are produced by a sprinkler nozzle located on the top of the tower. The particle size distribution can be evaluated by sampling the particles that solidify on the granulation tower floor (Gezerman, 2020). Mono-dispersed granules can be obtained by operating the nozzle of the sprinkler in the Rayleigh jet breakdown regime, since a rapid transition to the crystalline state can cause disintegration of the particles (Saleh and Barghi, 2016). Attempts to delimit the regimes based on dimensionless numbers can be found in the literature, there are criteria for aircraft breakdown regimes found in the literature. In (Dumouchel, 2008) it is shown that these regimes are associated with typical values of the liquid Weber number We_L, the gaseous Weber number We_G and the Ohnesorge Oh number. The Weber number is a measure of the relationship between drag force and surface tension. The Ohnesorge number describes the relationship of viscous effects in the liquid and surface tension.

The Rayleigh jet rupture regime operates when the fluid velocity is large enough, but still low, this concept defines the relationship of the inertia of the liquid and the surface tension (Saleh, 2010). The liquid Weber number (salt), the gaseous Weber number (air) and the Ohnesorge number will be:

$$We_l = \frac{\rho_l \cdot d \cdot u_l^2}{\sigma} > 8 \qquad \text{(eq. 1)}$$

$$We_a = \frac{\rho_a \cdot d \cdot (u_l - v_a)^2}{\sigma} < 0.4 \qquad \text{(eq. 2)}$$

Where, d is the diameter of the particle, σ is the surface tension of the liquid, ρ_l, ρ_a, are the density of the liquid and air respectively, u_l, v_a are the velocities of the liquid (particles) and air respectively. On the other hand:

$$Oh = \frac{\mu_l}{\sqrt{\rho_l \cdot d \cdot \sigma}} \qquad \text{(eq. 3)}$$

In addition, secondary disintegration is performed when:

$$\frac{We_a}{Re} \geq 0.2 \qquad \text{(eq. 4)}$$

3. Mathematical models

3.1. Mathematical model of the airflow inside the tower

For this study, the Ansys Fluent 18.1 Computational Fluid Dynamics (CFD) package is used, which is solved using a Eulerian approach. Computational fluid dynamics (CFD) modeling is used to investigate fluid flow patterns and fluid and particle trajectories under steady-state operating conditions. Airflow is modeled using the Eulerian approach, where turbulence is treated with Reynolds' averaged Navier-Stokes equations (RANS (Saleh, Barghi, 2016). Unlike other approaches to CFD methods that solve macroscopic property conservation equations, on the other hand, the Lattice-Boltzman (LBM) method describes the behavior of fluids on a mesoscopic scale (Dietzel and Sommerfeld, 2013). The Reynolds equations - Navier - Stokes Average (RANS) and the RNG k - ε model are presented below. (Saleh and Barghi, 2016)

$$\frac{\partial \rho}{\partial t} + \nabla \cdot (\rho \vec{u}) = 0 \qquad \text{(eq. 5)}$$

$$\frac{\partial \rho \vec{u}}{\partial t} + \nabla \cdot (\rho \vec{u}\vec{u}) = -\nabla p + \nabla \cdot \left(\mu_{eff}(\nabla \vec{u} + (\nabla \vec{u})^T)\right) \qquad \text{(eq. 6)}$$

$$\frac{\partial \rho \kappa}{\partial t} + \nabla \cdot (\rho \kappa \vec{u}) = \nabla \cdot (\alpha_\kappa \mu_{eff} \nabla \kappa) + G_\kappa - \rho_\varepsilon \qquad \text{(eq. 7)}$$

$$\frac{\partial \rho \varepsilon}{\partial t} + \nabla \cdot (\rho \varepsilon \vec{u}) = \nabla \cdot (\alpha_\varepsilon \mu_{eff} \nabla_\varepsilon) + C_1 \frac{\varepsilon}{\kappa} G_\kappa - C_2 \rho \frac{\varepsilon^2}{\kappa} \qquad \text{(eq. 8)}$$

These equations represent the conservation equations of momentum and mass, which are used by the CFD solver (Wang et al., 2021). On the other hand, the turbulent viscosity will be:

$$\mu_t = \rho \cdot C_\mu \cdot \left(\frac{\kappa^2}{\varepsilon}\right) \qquad \text{(eq. 9)}$$

Where, ε; is the dissipation rate (m^2/s^3); κ; is the turbulent kinetic energy (m^2/s^2) and Cμ is a constant. The effective viscosity shall be:

$$\mu_{eff} = \mu + \mu_t \qquad \text{(eq. 10)}$$

Where: α_κ, α_ε are the turbulent Prandtl numbers; G_κ is the turbulent kinetic energy (kg/m s^3) and C_1, C_2 are constant

3.2. Mathematical model of particles

In the analysis of salt particles, they are carried out from a Lagrangian trajectory approach using the Ansys Fluent 18.1 package using a CFD-DPM coupling. The different forces (viscous drag, lift force, buoyancy, etc.) that act on the Lagrangian particles along their trajectories are taken into account, as well as a stochastic behavior of the surrounding turbulent flow (Zahari et al., 2018). A particle in a granular flow can have two types of motion: translational and rotational. During its motion, the particle can interact with its neighboring particles or walls and interact with the surrounding fluid, through which momentum and energy are exchanged. Strictly speaking, this motion is affected not only by forces and torques originated by its immediate neighboring particles and the neighboring fluid, but also by distant particles and fluids through the propagation of disturbing waves. (Zhu et al., 2007)

In the Lagrange frame of reference, the trajectory is predicted by integrating the balance of forces in it while it is analyzed as a discrete phase. This balance of forces equates the inertia of the particle with the forces acting on the particle described in the following equation:

$$m_{p,i} \cdot \frac{d\vec{v}_{p,i}}{dt} = m_{p,i} \cdot \vec{g} + \sum \vec{F_c} + \vec{F_f} \qquad \text{(eq. 11)}$$

$$\sum \vec{F_c} = \left(\vec{F_n} \cdot \vec{n_{ij}} - F_n \cdot n_{ij}\right) + \left(\vec{F_t} \cdot \vec{t_{ij}} - F_t \cdot t_{ij}\right) \qquad \text{(eq. 12)}$$

$$I_{p,i} \cdot \frac{d\,\vec{\omega}_{p,i}}{dt} = \sum \vec{T_i} \qquad \text{(eq. 13)}$$

Where $m_{p,i}\,\vec{g}$ represents the gravity of the particle, $\vec{F_f}$ is the total force of the fluid on each particle, $I_{p,i}$ is the rotational inertia of the particle, $\sum \vec{T_i}$ is the total torque acting on the particle, $\vec{v}_{p,i}$ is the linear velocity, $\vec{\omega}_{p,i}$ is the angular velocity of the particle, $\vec{n}_{ij}$ is the normal direction from the center of the particle i al of the particle j; $\sum \vec{F}_c$ is the total contact force on each particle and is calculated using the Hertz-Mindlin model (no slip) (Wang et al., 2021). For a fine particle system, non-contact forces such as van der Waals and electrostatic forces must also be included. (Zhu et al., 2007)

3.3. CFD-DPM coupling

The numerical models of particle-fluid flows can be categorized into three methods, according to the treatment of the particles and the fluid phases: Eulerian-Eulerian methods, Lagrangian-Lagrangian methods and Eulerian-

Lagrangian methods. In Eulerian-Eulerian methods, both the fluid phase and the particle phase are defined as continuous interpenetrated phases. A discrete phase model (DPM) is used in the Lagrangian frame of reference to track the movement of the particles, while a Eulerian formulation is used simultaneously for the continuous phase. The different forces (viscous drag, lift force, buoyancy, etc.) that act on the Lagrangian particles along their trajectories are taken into account, as well as a stochastic behavior of the surrounding turbulent (Zahari et al., 2018). For this work an Eulerian-Lagrangian approach is established, where the gas phase (air) is treated by means of a Eulerian approach and the discrete phase (particles) by a Lagrangian approach, the model is solved using the Ansys Fluent 18.1 software by means of a coupling. CFD-DPM. The drag force can be described by a constitutive equation defined as: (Cooper and Coronella, 2005)

$$F_D = \frac{3 \cdot \mu \cdot C_D \cdot Re_p}{4 \cdot \rho_p \cdot d^2} \qquad \text{(eq. 14)}$$

Where: μ is the viscosity of the particle (kg/m s); C_D is the drag coefficient of the particle; Re_p is the Reynolds number of the particle, and ρ_p is the density of the particle (kg/m^3). On the other hand, although the air velocity in prilling towers ranges between approximately 1.37 and 2.45 m/s depending on the geometry of the tower and the air flow (Saleh and Barghi, 2016), for a stable airflow and the reduction of particle drag an air velocity of 1.0 m/s is recommended at a small Reynolds number ($Re_{p)}$. The range of Reynolds number and drag coefficient correlations ($C_{D)}$has been described for three regions: the Stokes law region ($Re_p < 0.3$), the intermediate region ($0.3 < Re_p < 500$), and Newton's law region ($500 < Re_p < 2 \times 10^5$). In the intermediate region, the drag coefficient is given as a function of the Reynolds number of the particle:

$$C_D = \left(\frac{24}{Re_p}\right)\left(1 + 0.14 \cdot Re_p^{0.687}\right) \qquad \text{(eq. 15)}$$

Where:

$$Re_p = \frac{\rho_a \cdot d \cdot (u_p - v_a)}{\mu_a} \qquad \text{(eq. 16)}$$

Where: u_p is the velocity of the particle (m/s); v_a is the air velocity (m/s) and μ_a is the viscosity of the air (kg/m s).

4. Numerical modeling

4.1. Model validation

The study is carried out using the Ansys Fluent R18.1 package, using a CFD-DPM coupling model, where the gas phase is treated from a Eulerian approach, while the discrete phase from a Lagrangian approach. In Fig. 2 the configuration of the geometry is shown using the Ansys SpaceClaim Direct Modeler package, the dimensions of the tower are given in Tab. 2.

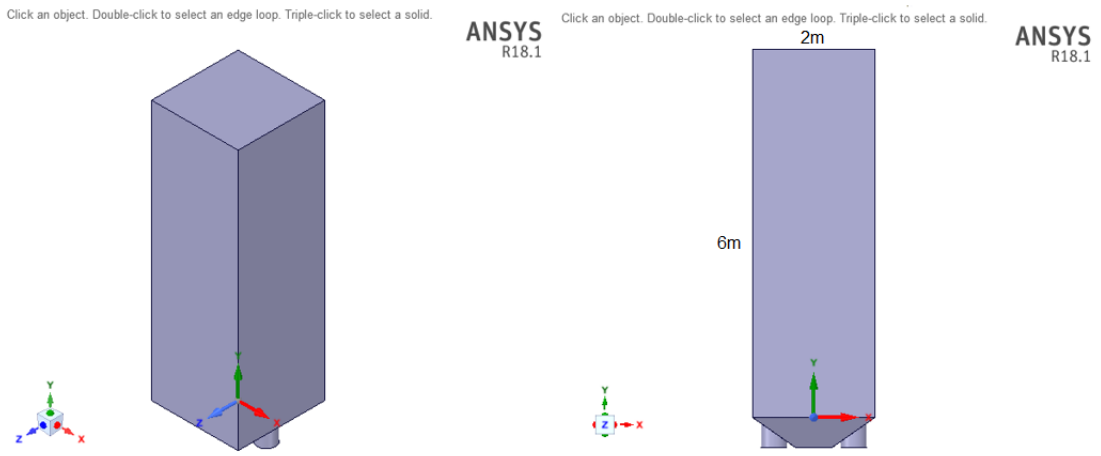

Fig. 2: Geometry Settings

The geometry is meshed using the Ansys Meshing PrePost environment, with an element size of 0.008m, a curvature-type size function, and inflation controlled by the program (Fig. 3). The grid has 108,258 nodes and 442,269 elements.

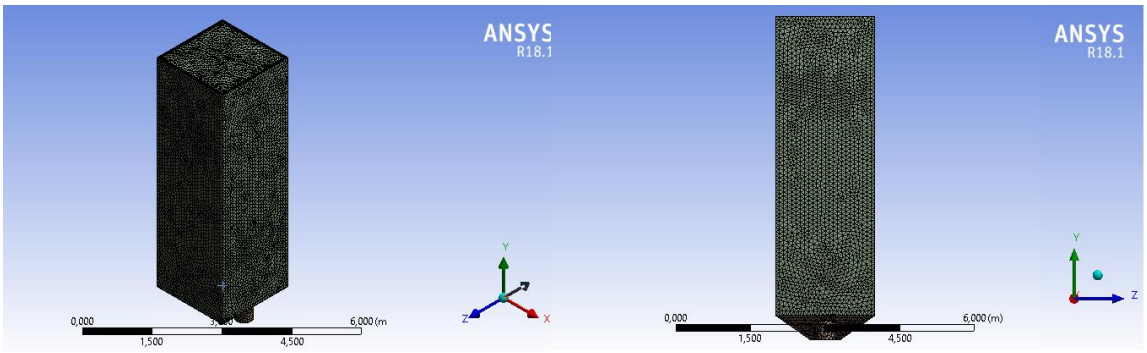

Fig. 3: Mesh configuration

In the processing stage, a double precision study is considered in a permanent regime considering the effect of gravity (9.81m/s), in addition, the two analysis models are defined for each phase. Turbulence is treated with the RNG k-epsilon model, while the discrete phase is simulated using a DPM model with an injection of particles at a rate of 0.0094kg/s and a velocity of 9.161m/s. The size of the particles is variable and ranges from 0.0000788mm to 0.5mm.

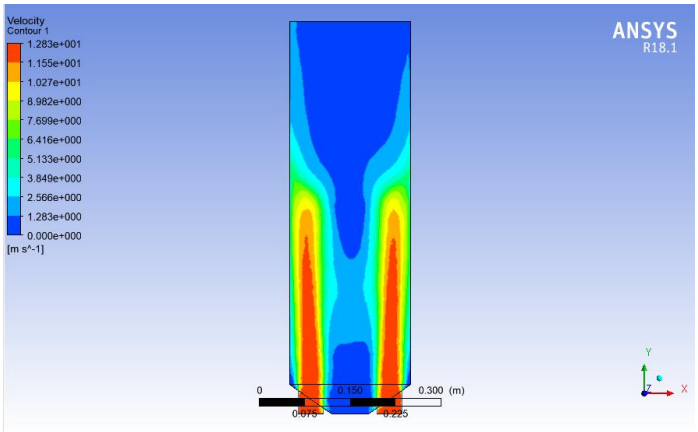

Fig. 4: CFD post processing

The Post-processed stage is analyzed using CFD-Post (Fig. 4) in which an XY sample plane is defined due to the symmetry of the tower, to analyze the air flow inside the tower.

5. Results and discussion

In this section we analyze the speed curves of the air ascent into the tower (velocity v of the Y axis) and the speed curve of the fall of the particles along the Y axis. Fig. 6 shows the diagram of air speed that goes from the base of the tower (12.5 m/s) to the top, in which a speed of approximately 1m/s is observed, which is within the ranges established in prilling towers. In addition, a significant decrease in the curve is observed when the air reaches half the height of the tower, due to the interaction with the salt particles.

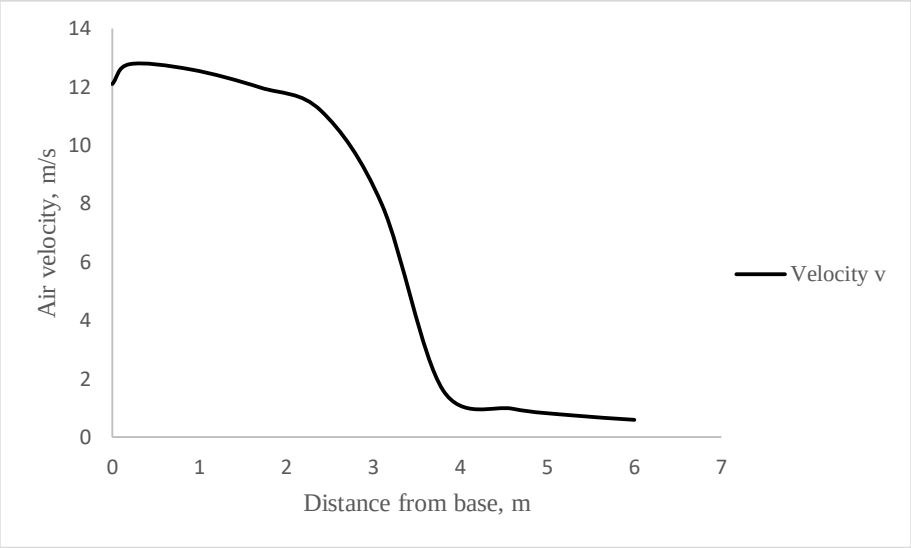

Fig. 5: Variation of the rate of ascent of the air

On the other hand, the variation of the speed of fall of the particle is observed in Fig. 6, where there is an initial speed of 9,161 m / s which is the speed at which the jet leaves the sprinkler, it is also appreciated that the speed stabilizes (speed limit) approximately 3m from the height of the tower. Reaching a value of approximately 4m/s.

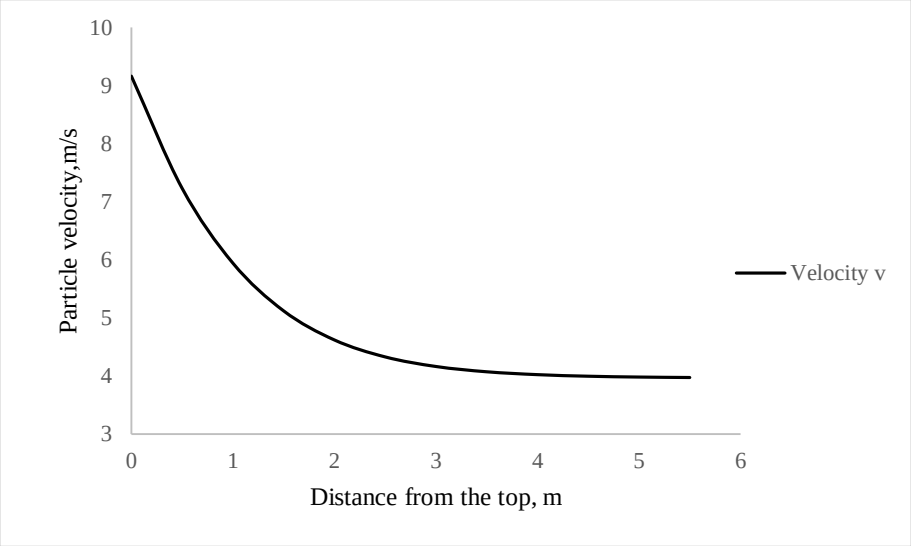

Fig. 6: Variation of the falling velocity of the particle

The limit or terminal velocity of the particle v_t can be determined as a function of the height of the tower according to the following equation: (Saleh and Barghi, 2016):

$$v_t = \sqrt{\frac{4}{3} \cdot \frac{d_p \cdot g \cdot (\rho_p - \rho_a)}{C_D \cdot \rho_a}} \qquad \text{(ec. 17)}$$

This speed is the result of Newton's Law, which establishes that if a spherical particle is dropped into a fluid, it acquires an accelerated movement until it reaches a constant final speed, called the limit speed of fall or terminal speed. On the other hand, the analysis of the distribution of the number of particles inside the tower shows according to Fig. 7 shows that droplets of size between 9.14 µm and 22.7 µm prevail in a percentage range of between 5% and 27%.

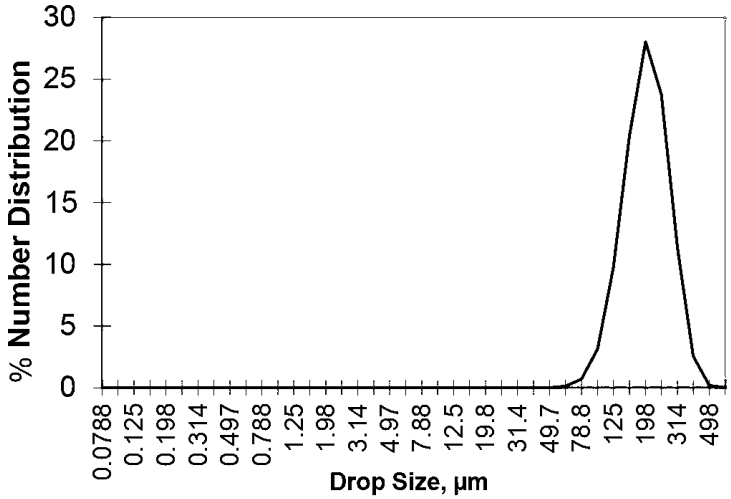

Fig. 7: Particle distribution number

On the other hand, the same range of particles occupy the largest area in the lower part of the tower, representing 30% of the area occupied by particles of this size (Fig. 8).

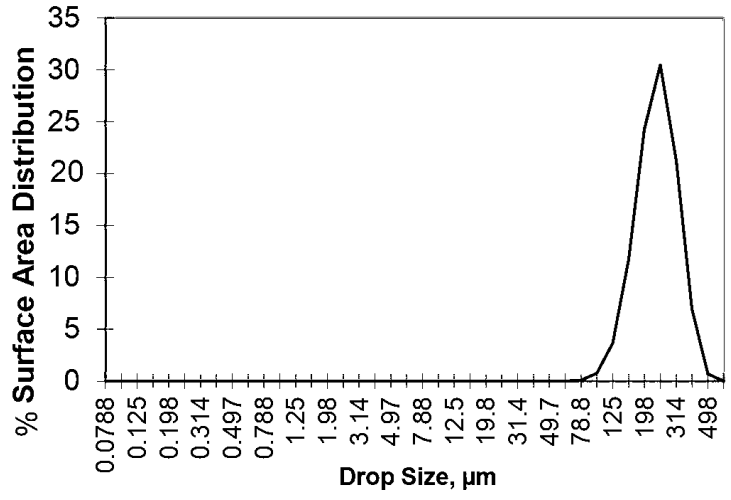

Fig. 8: Surface area distribution

The volume of distribution of particles can be observed in Fig. 9 where those that occupy the largest volume are the largest particles, as well as what is shown in Fig. 10 which represents the accumulated volume that contrasts the values of particle sizes prevailing of 9.14µm and 22.7µm. However, the maximum value of particle size which is 500µm or 0.5mm is the one considered to analyze the particle in a Lagrangian way.

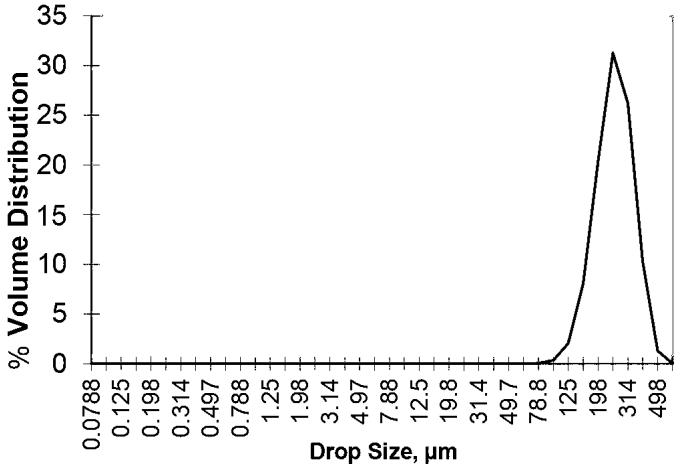

Fig. 9: Volume distribution

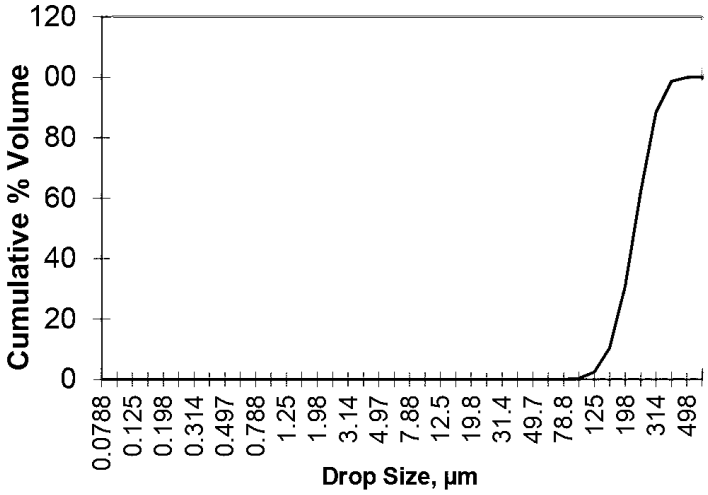

Fig. 10: Cumulative % volume

6. Conclusions

The CFD-DPM simulation was carried out inside the molten salt prilling tower. Where the gas phase (air) was considered from the Eulerian point of view and the discrete phase (solar salt particles) from the Lagrangian point of view. The analysis of the variation in the speed of the circulating air inside the prilling tower shows that it has a significant decrease from the 3m height of the tower, reaching an almost constant value of 1m / s. At that point it begins to stabilize due to the interaction of the air with the salt particles. On the other hand, the discrete analysis of the particles shows that it acquires a terminal velocity of 4m / s from a height of 3m, which in the same way is due to the interaction with the fluid (air) in countercurrent.

During the modeling of particles inside the tower, it was observed that the particles that prevail in the particle-particle and particle-air interactions are the largest, in addition it is observed that these particles occupy a greater surface area within the gaseous medium as well as a higher volume. This is because the smallest particles are carried through the air into the environment in the form of aerosols. On the other hand, the size and configuration of the tower, as well as the configuration of the atomization process of the molten material, have an important significance in the distribution of particles inside the tower, as well as in the behavior of the air flow. Although the results of this study are specific to a tower of specific interest, the process can be extrapolated to similar or larger-scale cases.

7. References

Cooper, S., and Coronella, C. J. 2005. CFD simulations of particle mixing in a binary fluidized bed. Powder Technology, 151(1–3), 27–36. https://doi.org/10.1016/J.POWTEC.2004.11.041

Dietzel, M., and Sommerfeld, M. 2013. Numerical calculation of flow resistance for agglomerates with different morphology by the Lattice–Boltzmann Method. Powder Technology, 250, 122–137. https://doi.org/10.1016/J.POWTEC.2013.09.023

Dumouchel, C. 2008. On the experimental investigation on primary atomization of liquid streams. Experiments in Fluids 2008 45:3, 45(3), 371–422. https://doi.org/10.1007/S00348-008-0526-0

Gezerman, A. O. 2020. Mathematical modeling for prilling processes in ammonium nitrate production. Engineering Reports, 2(6), e12173. https://doi.org/10.1002/ENG2.12173

Mehos, M., Turchi, C., Vidal, J., Wagner, M., Ma, Z., Ho, C., Kolb, W., Andraka, C., and Kruizenga, A. 2017. Concentrating Solar Power Gen3 Demonstration Roadmap. Nrel/Tp-5500-67464, 1–140. https://doi.org/10.2172/1338899

Nissen, D. A. 1980. Thermophysical properties of the equimolar mixture NaNO/sub 3/-KNO/sub 3/ from 300 to 600/sup 0/C. https://doi.org/10.2172/6765587

Paz-Paredes, I., Barbosa-Saldaña, J. G., Arce-Medina, E., Moreno-Pacheco, L. A., and Quinto-Diez, P. 2017. Análisis numérico de la hidrodinámica y la transferencia de calor del flujo gas-sólidos en dos configuraciones de salida de un riser industrial usando la teoría meso-escala para predecir el arrastre interfacial. Revista Internacional de Métodos Numéricos Para Cálculo y Diseño En Ingeniería, 33(3–4), 155–163. https://doi.org/10.1016/J.RIMNI.2016.04.002

Ricardo, G. A. N., Noriler, D., Martignoni, W. P., and Meier, H. F. 2013. Eulerian-lagrangian analysis of multiphase flow in urea prilling process with phase changing. Chemical Engineering Transactions, 32, 2173–2178. https://doi.org/10.3303/CET1332363

Saleh, S. N. 2010. BASIC CONCEPTS OF PRILLING TOWER DESIGN. The International Conference on Chemical and Environmental Engineering, 5(5th International Conference on Chemical and Environmental Engineering), 1–17. https://doi.org/10.21608/ICCEE.2010.37380

Saleh, S. N., and Barghi, S. 2016. Reduction of fine particle emission from a prilling tower using CFD simulation. Chemical Engineering Research and Design, 109, 171–179. https://doi.org/10.1016/J.CHERD.2016.01.017

Wang, X., Yao, J., Gong, L., Li, Y., Yang, Y., and Zhao, H. 2021. Computational fluid dynamic–discrete element method coupling analysis of particle transport in branched networks. Particuology, 55, 140–150. https://doi.org/10.1016/J.PARTIC.2020.05.005

Zahari, N. M., Zawawi, M. H., Sidek, L. M., Mohamad, D., Itam, Z., Ramli, M. Z., Syamsir, A., Abas, A., and Rashid, M. 2018. Introduction of discrete phase model (DPM) in fluid flow: A review. AIP Conference Proceedings, 2030. https://doi.org/10.1063/1.5066875

Zhu, H. P., Zhou, Z. Y., Yang, R. Y., and Yu, A. B. 2007. Discrete particle simulation of particulate systems: Theoretical developments. Chemical Engineering Science, 62(13), 3378–3396. https://doi.org/10.1016/J.CES.2006.12.089